



OPEN

## Structural optimization and performance analysis of the cable-driven fine adjustment mechanism for the new FAST feed cabin

Lucong Zhang<sup>1,2</sup>, Jinghai Sun<sup>1,4</sup>✉, Peng Jiang<sup>1,4,5</sup> & Hui Li<sup>1,3,5</sup>

The Five-hundred-meter Aperture Spherical radio Telescope (FAST) is the world's largest and most sensitive single-dish radio telescope. To meet the growing demands of astronomical observations, the FAST team has proposed a new feed cabin configuration based on a cable-driven fine-tuning mechanism. This design replaces the traditional rigid A–B rotator and Stewart platform with a lightweight steel cable structure, significantly reducing the overall structural weight. To satisfy receiver installation requirements, enhance the payload capacity of the receiver platform, and maximize zenith angle coverage, this paper proposes a modeling approach tailored to the new configuration and conducts structural optimization under cable tension constraints. Simulation results demonstrate that the new configuration achieves a substantial improvement in payload capacity and extends the zenith angle to at least 50°, enabling FAST to accommodate a wider range of receivers and enhance sky coverage near the Galactic center. The proposed feed cabin design not only meets current scientific needs but also provides a robust technical foundation and feasible upgrade path for future expansion and array development of FAST.

The Five-hundred-meter Aperture Spherical radio Telescope (FAST) is currently the world's largest and most sensitive single-dish radio telescope (Fig. 1)<sup>1–3</sup>. Since its official commissioning in 2020, FAST has maintained stable and highly efficient observational performance, leading to a series of significant achievements in areas such as pulsar detection, fast radio burst (FRB) studies, and neutral hydrogen (HI) imaging<sup>4–9</sup>. These results not only validate the exceptional capabilities of FAST but also highlight its substantial scientific value in the field of radio astronomy.

As shown in Figs. 1 and 2, FAST consists of two major subsystems: the active reflector system and the feed support system. The active reflector system has more than 4000 triangle panels and a supporting cable-net structure, which enables dynamic focusing of radio waves through active surface deformation. The feed support system has six steel cables supported by six towers, forming a large-span parallel cable-driven mechanism that adjusts the position and orientation of the feed cabin. To ensure high-precision positioning of the receiver's feed inside the cabin, a fine adjustment mechanism is employed. First, an internal A–B rotator allows rotation about two orthogonal axes, compensating for tilt deviations caused by cabin movement. Second, a Stewart platform performs fine adjustments in real time to correct residual positioning errors, enabling the phase center of the feed to achieve a root-mean-square (RMS) positioning accuracy of 10 mm<sup>10–13</sup>.

As demonstrated in the early research by Yin et al<sup>14</sup>, the FAST feed support system is theoretically capable of achieving at least a 50° observational zenith angle through a feasible cabin attitude configuration scheme, which determines the cabin orientation via coordinated actuation of the cable-driven mechanism, the A–B rotator, and the Stewart platform. However, in actual operation, the current feed cabin houses rigid structures—the A–B rotator and the Stewart platform—with a combined weight of 10.1 tons, accounting for approximately 34% of the total cabin mass. This substantial load significantly increases cable tension during large zenith-angle observations. When the zenith angle approaches 40°, the cable tensions may exceed the system's safety thresholds, triggering protection mechanisms and potentially interrupting observations. To address this challenge, a new feed cabin structure is urgently required. Instead of the previous A–B rotator and Stewart platform assembly, the new

<sup>1</sup>National Astronomical Observatories, Chinese Academy of Sciences, Beijing 100012, China. <sup>2</sup>University of Chinese Academy of Science, Beijing 100049, China. <sup>3</sup>CAS Key Laboratory of FAST, National Astronomical Observatories, Beijing 100020, China. <sup>4</sup>Guizhou Radio Astronomical Observatory, Guiyang 550000, China. <sup>5</sup>These authors contributed equally to this work: Peng Jiang and Hui Li. ✉email: sjh@nao.cas.cn

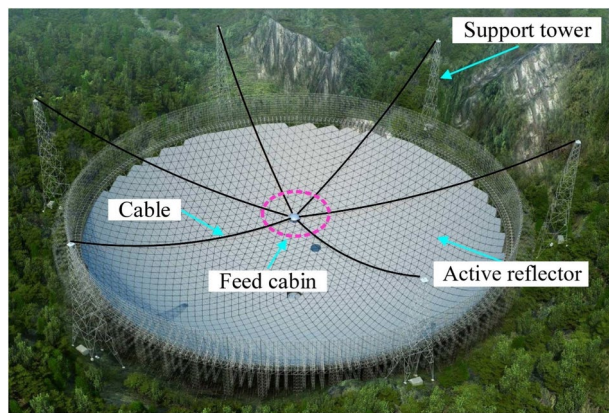


**Fig. 1.** Overall view of the FAST structure.

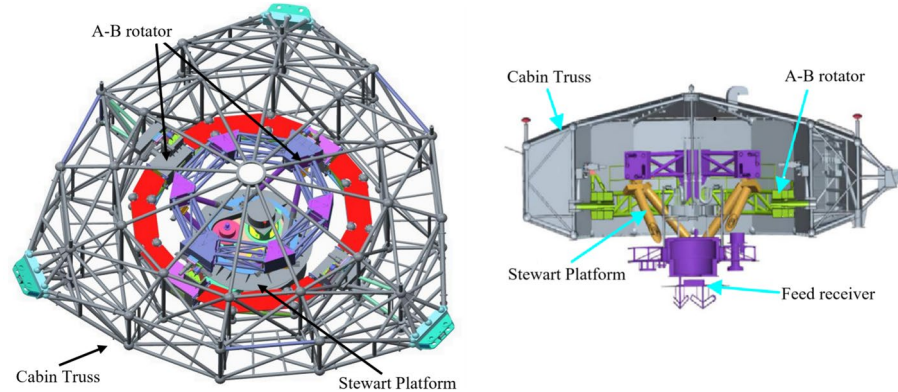


**Fig. 2.** Schematic diagram of the feed cabin structure.

design adopts a lightweight cable-driven mechanism, which reduces the mass share of the support system and increases the proportion of usable payload. This would not only enable the integration of more receivers, but also allow the system to safely achieve zenith angles of  $50^\circ$  or higher, thereby expanding FAST's sky coverage toward the Galactic center.

To meet these demands, Yao et al<sup>15</sup> proposed a feed cabin configuration, as shown in Fig. 4(a) which replaces the original A-B rotator and Stewart platform with a system based on guide rails, pulley mechanisms, and flexible steel cables. This design significantly reduces the overall structural mass. However, since the receiver layout scheme for the new feed cabin as shown in Fig. 3 and had not yet been proposed at that time, the structural design was not optimized based on the actual distribution of receivers. Therefore, this study focuses on the structural optimization and performance analysis of the fine-tuning mechanism under the receiver configuration requirements.

Since the guide rail and pulley structures in the new cable-driven fine-tuning system of the feed cabin have been partially modeled and analyzed in<sup>15</sup>, this paper does not repeat those details. Instead, the mechanism is simplified, as shown in Fig. 4(b), the design replaces the original guide rail and pulley components with winches, anchor points, and steel cables. In the optimization process, system-level analysis of cable tension distribution and structural performance is conducted under the new configuration. With the receiver layout now specified, the new configuration faces several critical challenges, including: optimizing structural parameters under cable tension equilibrium; avoiding mechanical interference and collisions while maximizing the zenith observation angle; and ensuring system stability and reliability under large inclination conditions.

To evaluate the feasibility and advantages of this structure, it is essential to establish a complete geometric and mechanical model to reveal the coupling between cable tension and platform posture. Constrained optimization of key design parameters under cable tension limits is also required to ensure high stability of the feed cabin during astronomical observations. Given the relatively low operating speed of the feed cabin within its workspace ( $0\text{--}24\text{ mm/s}$ )<sup>14</sup>, its structural behavior is primarily governed by static effects. Therefore, the system can reasonably be treated as a quasi-static structure in the modeling process. A static analysis approach is adopted to evaluate cable tension distribution, structural posture stability, and sensitivity to key parameters. The main contributions of this study include the following three aspects:

1. Establish static and kinematic models of the new feed cabin, then analyze its loading conditions under operational scenarios, thereby ensuring structural safety.

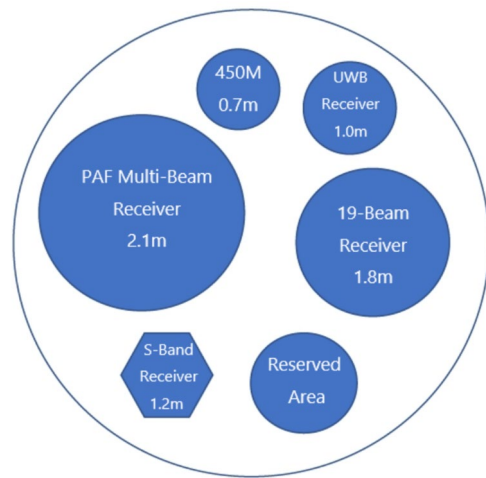


**Fig. 3.** Schematic diagram of receiver platform layout.

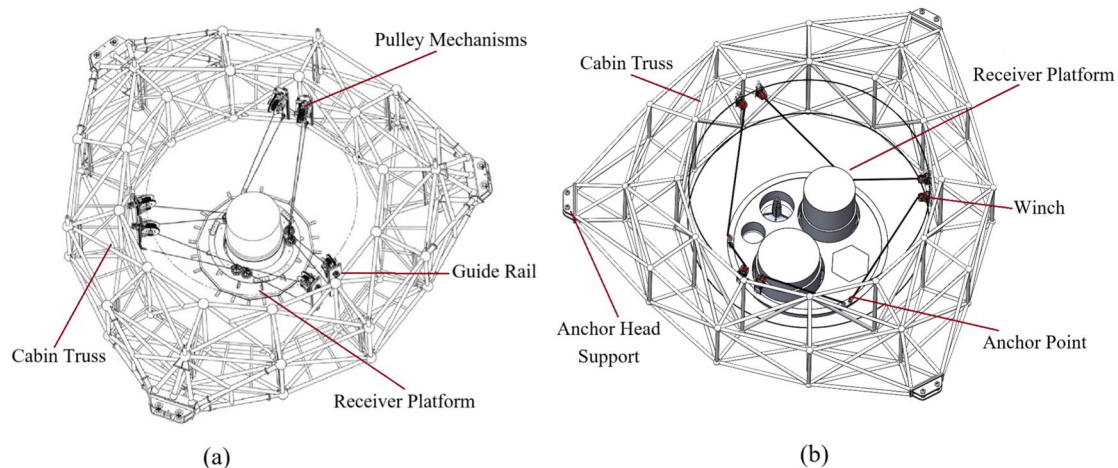


**Fig. 4.** New feed cabin configuration. (a) Original system with the cabin truss, guide rails, pulley mechanisms, and the receiver platform. (b) Simplified cable-driven model with six winches and six anchor points mounted on the truss to control the receiver platform.

2. Maximize the achievable zenith angle of the feed cabin as the optimization objective, with multiple constraints imposed—such as spatial structural dimensions, allowable tension range for individual cables, and overall tension balance. Key structural parameters are then optimized accordingly.

3. Perform collision detection under extreme working conditions based on the optimized structure, ensuring that no collision occurs between the cables and receivers when the feed cabin operates near its mechanical limits.

This study focuses on the conceptual design stage, aiming to investigate the global influence of key structural parameters on the feed cabin's kinematic and mechanical behavior. A rigid-body cable-driven model is adopted to efficiently capture the coupling between cable tension and platform motion while allowing full-parameter exploration with controllable computational cost. The modeling framework is designed to be extendable and upgradable; in subsequent phases, it will be refined to include flexible components, detailed mass distributions, and FEM-based validation of the optimized structure. This progressive development ensures that the early-stage analysis remains physically consistent and directly supports the detailed engineering design of the feed cabin system.

This paper is structured as follows: Section "Structural design and coordinate system of the new feed cabin configuration" describes the structural design of the new feed cabin configuration and establishes the corresponding coordinate systems. Section "Kinematic and static modeling of the new feed cabin structure" derives the mechanical model of the system. In Section "Structural parameter optimization and performance validation", structural parameters are optimized under specific constraints, and the performance of the optimized model is evaluated. Section "Tilt and payload performance validation of the feed cabin system" carries out collision detection to verify the feasibility of the new configuration under real working conditions. Finally, Section "Conclusion" concludes the study with a summary of the research outcomes.

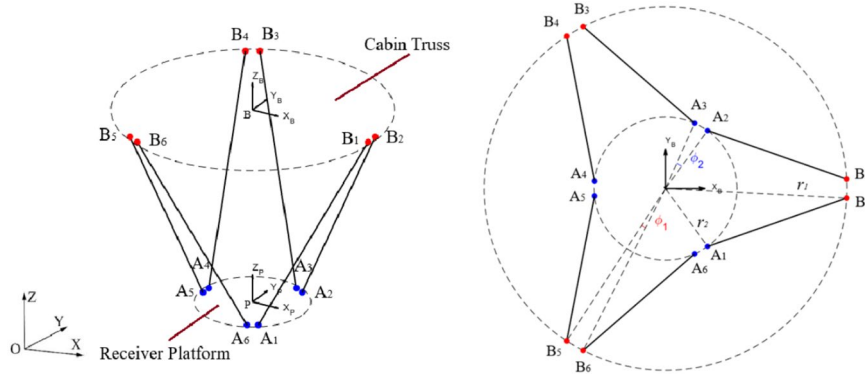


**Fig. 5.** Spatial distribution of winches and anchor points.

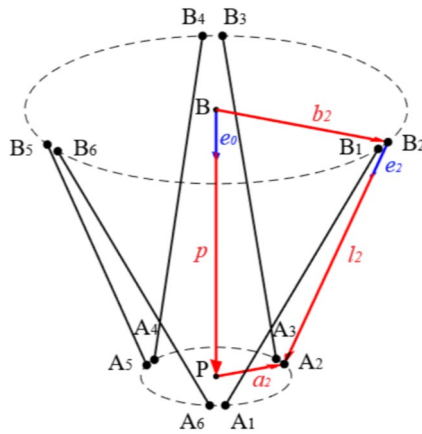


**Fig. 6.** Vector diagram of the new feed cabin.

## Structural design and coordinate system of the new feed cabin configuration

### Description of the new configuration

The design of the new feed cabin aims to optimize the structural configuration, enabling a broader observational range and reduced overall weight while ensuring high-precision and safe operation. This configuration employs six flexible cables to directly drive the receiver platform, eliminating the original rigid A-B rotator and the Stewart platform. As a result, the mechanical structure of the system is simplified.

As shown in Fig. 5, the winches are arranged in pairs on the cabin truss, with their height aligned with the geometric center of the truss. They are sequentially labeled as  $B_i$  ( $i = 1 \sim 6$ ). The cable anchor points on the receiver platform are defined as  $A_i$  ( $i = 1 \sim 6$ ). The winches are positioned along a circular path on the cabin truss with a distribution radius of  $r_1$ , while the anchor points on the receiver platform are arranged along a separate circle with a radius of  $r_2$ . The three pairs of winches and anchor points are evenly spaced at  $120^\circ$  intervals around their respective circles. In each group, the included angle between two adjacent winches is denoted as  $\varphi_1$ , and the angle between two anchor points is denoted as  $\varphi_2$ .

### Definition of coordinate systems

To describe the motion and orientation of the new feed cabin, three coordinate systems are established, as illustrated in Fig. 5:

1. The global coordinate system  $\{O-X_Y_Z\}$  is fixed to the terrestrial reference frame and is used to describe the overall spatial position and orientation of the feed cabin.
2. The cabin truss coordinate system  $\{B-X_B Y_B Z_B\}$  is fixed to the geometric center of the truss and is used to describe the orientation changes of the cabin truss and its associated mechanisms.
3. The receiver platform coordinate system  $\{P-X_P Y_P Z_P\}$  is fixed at the geometric center of the receiver platform and is used to describe its orientation changes.

The unit vectors for the cabin truss are denoted as  $e_{Bx}$ ,  $e_{By}$ , and  $e_{Bz}$ , and the unit vectors for the receiver platform are denoted as  $e_{Px}$ ,  $e_{Py}$ , and  $e_{Pz}$ .

### Description of position and orientation

As shown in Fig. 6, the position vector of point  $P$  from the geometric center of the cabin truss  $B$  is denoted as  $p$ , with the corresponding unit vector  $e_0$ . The position vector of winch  $B_i$  relative to the center  $B$  is denoted as  $b_i$ ,

and the position vector of anchor point  $A_i$  relative to the geometric center of the receiver platform  $P$  is denoted as  $\mathbf{a}_i$ . The vector from anchor point  $A_i$  to winch  $B_i$  is denoted as  $\mathbf{l}_i$ , with the corresponding unit direction vector  $\mathbf{e}_i$ .

Here,  $\mathbf{p}$ ,  $\mathbf{b}_i$ ,  $\mathbf{a}_i$ , and  $\mathbf{l}_i$  denote vectors expressed in the global coordinate system  $\{O\}$ , whereas  ${}^B\mathbf{B}_i$  and  ${}^P\mathbf{A}_i$  represent the coordinates of points  $B_i$  and  $A_i$  expressed in the local coordinate systems  $\{B\}$  and  $\{P\}$ , respectively.

The angular transformations defining the orientations of the local frames are described using an intrinsic Z-Y-X Euler rotation sequence. All coordinate systems are initially aligned. The orientation of the cabin truss frame  $\{B\}$  relative to the global frame  $\{O\}$  is obtained by applying an intrinsic rotation about  $Z_B$  by  $\alpha_1$ , followed by a rotation about the updated  $Y_B$  by  $\beta_1$ , and then about the updated  $X_B$  by  $\gamma_1$ .

Similarly, the orientation of the receiver platform frame  $\{P\}$  relative to the cabin truss frame  $\{B\}$  is obtained through an intrinsic rotation about  $Z_P$  by  $\alpha_2$ , then about the updated  $Y_P$  by  $\beta_2$ , and finally about the updated  $X_P$  by  $\gamma_2$ . The rotation matrices about the  $x$ ,  $y$ , and  $z$  axes are denoted as  $R_x$ ,  $R_y$ , and  $R_z$ .

Based on this definition, the rotation matrix from the cabin truss coordinate system  $\{B\}$  to the global coordinate system  $\{O\}$  is given by

$${}^O\mathbf{R} = R_z(\alpha_1) R_y(\beta_1) R_x(\gamma_1).$$

The rotation matrix from the receiver platform coordinate system  $\{P\}$  to the cabin truss coordinate system  $\{B\}$  is given by

$${}^P\mathbf{R} = R_z(\alpha_2) R_y(\beta_2) R_x(\gamma_2).$$

Finally, the rotation matrix from the receiver platform coordinate system  $\{P\}$  to the global coordinate system  $\{O\}$  is obtained as

$${}^O\mathbf{R} = {}^P\mathbf{R} \cdot {}^B\mathbf{R}.$$

In the previous work<sup>14</sup>, the FAST team defined the coordinates of winch  $B_i$  in the cabin truss coordinate system  $B$  as follows:

$${}^B\mathbf{B}_i = [r_1 \cos\left(\frac{2\pi}{3} \cdot \lfloor \frac{i-1}{2} \rfloor + (-1)^i \frac{\varphi_1}{2}\right) \quad r_1 \sin\left(\frac{2\pi}{3} \cdot \lfloor \frac{i-1}{2} \rfloor + (-1)^i \frac{\varphi_1}{2}\right) \quad 0]^T, \quad (1)$$

the coordinates of anchor point  $A_i$  in the receiver platform coordinate system  $\{P\}$  are defined as:

$${}^P\mathbf{A}_i = [r_2 \cos\left(\frac{2\pi}{3} \cdot \lfloor \frac{i-1}{2} \rfloor + (-1)^i \cdot \frac{2\pi/3 - \varphi_2}{2}\right) \quad r_2 \sin\left(\frac{2\pi}{3} \cdot \lfloor \frac{i-1}{2} \rfloor + (-1)^i \cdot \frac{2\pi/3 - \varphi_2}{2}\right) \quad 0]^T. \quad (2)$$

where  $i = 1 \sim 6$ ,  $f(x) = \lfloor x \rfloor$  denotes the floor function, which represents the greatest integer less than or equal to  $x$ . Assuming that the origin of the cabin truss coordinate system coincides with the origin of the global coordinate system, the coordinate relationships can be derived as follows: the origin of the receiver platform coordinate system expressed in the cabin truss coordinate system is denoted as  ${}^B\mathbf{p}$ , and its coordinates in the global coordinate system are given by  ${}^O\mathbf{R} \cdot {}^B\mathbf{p}$ . The coordinates of the cabin truss point  $B_i$  in the global coordinate system are expressed as  ${}^O\mathbf{R} \cdot {}^B\mathbf{b}_i$ .

By combining the coordinates of the winches and the anchor points, along with the rotation matrices between the coordinate systems, the position of the anchor point  $A_i$  in the cabin truss coordinate system can be derived as:

$${}^B\mathbf{A}_i = {}^B\mathbf{p} + {}^P\mathbf{R} \cdot {}^P\mathbf{a}_i. \quad (3)$$

The position of the anchor point  $A_i$  in the global coordinate system is:

$$\mathbf{A}_i = {}^O\mathbf{R} \cdot {}^B\mathbf{p} + {}^O\mathbf{R} \cdot {}^P\mathbf{a}_i. \quad (4)$$

This section describes the structural configuration of the new feed cabin and introduced the coordinate systems, providing a unified framework to describe the spatial position and orientation of the feed cabin. This forms the theoretical foundation for the subsequent modeling and optimization.

## Kinematic and static modeling of the new feed cabin structure

### Kinematic model

Based on the modeling and analysis method of the external cable-driven mechanism proposed by Yin et al<sup>16</sup>, the kinematic relationships of the system are derived by establishing vector loop equations. For the  $i$ -th cable driving the receiver platform, a closed-loop vector equation is formulated to describe the displacement relationships among key points.

As shown in Fig. 6, the vector  $\mathbf{l}_i$  corresponding to any cable can be expressed as:

$$\mathbf{l}_i = \mathbf{p} - \mathbf{b}_i + \mathbf{a}_i \quad (5)$$

All vectors in Equation (5), including  $\mathbf{p}$ ,  $\mathbf{b}_i$ , and  $\mathbf{a}_i$ , are expressed in the world coordinate frame  $\{\mathcal{O}\}$  to ensure a consistent kinematic representation.

Therefore, the unit direction vector of any cable is given by  $\mathbf{e}_i = \mathbf{l}_i / |\mathbf{l}_i|$ .

Since the angular velocity  ${}^O\omega_P$  of the receiver platform is influenced by the angular velocity  ${}^O\omega_B$  of the cabin truss, the angular velocity of the receiver platform in the world frame can be decomposed as follows:

$${}^O\omega_P = {}^O\omega_B + {}_B^O\mathbf{R} {}^B\omega_P \quad (6)$$

When the cabin truss orientation is treated as fixed and the winch and anchor positions are structurally constant, the receiver platform moves solely through cable length actuation. In this case,  ${}^O\omega_B = \mathbf{0}$ , and  ${}^O\omega_P = {}_B^O\mathbf{R} {}^B\omega_P$ . Letting  $C(\boldsymbol{\omega})$  denote the cross-product (or skew-symmetric) matrix of the angular velocity vector  $\boldsymbol{\omega}$ .

By transforming Equation (5) into the global coordinate system and differentiating both sides, multiplying both sides by the unit direction vector  $\mathbf{e}_i$ , and arranging in matrix form, this yields:

$$\dot{\mathbf{l}}_i = \mathbf{e}_i \cdot {}_B^O\mathbf{R} \cdot {}^B\dot{\mathbf{l}}_i = [\mathbf{e}_i \quad C(\mathbf{a}_i)\mathbf{e}_i] \begin{bmatrix} {}_O\dot{\mathbf{p}} \\ {}^O\omega_P \end{bmatrix} \quad (7)$$

Let  $\mathbf{L} = [l_1 \quad \dots \quad l_6]^T$  denote the vector of cable lengths. Taking the time derivative yields  $\dot{\mathbf{L}}$ , representing the velocity vector of each cable. Based on this, the inverse Jacobian matrix can be constructed, establishing the kinematic relationship between the cable velocities and the velocity of the receiver platform.

$$\dot{\mathbf{L}} = \mathbf{J} \mathbf{q}.$$

The combined vector of the translational and angular velocities of the receiver platform is defined as  $\mathbf{q} = \begin{bmatrix} \dot{\mathbf{p}} \\ {}^O\omega_P \end{bmatrix}$ , and the inverse Jacobian matrix  $\mathbf{J}$  can be expressed as:

$$\mathbf{J} = \begin{bmatrix} \mathbf{e}_1 & \dots & \mathbf{e}_6 \\ C(\mathbf{a}_1)\mathbf{e}_1 & \dots & C(\mathbf{a}_6)\mathbf{e}_6 \end{bmatrix}^T.$$

### Static analysis

Under static equilibrium conditions, the tension forces and the corresponding moments exerted by the cables on the receiver platform are considered. Let  $t_i$  denote the scalar tension in the  $i$ -th cable, and let the corresponding force vector acting on the receiver platform be

$$\mathbf{f}_i = -t_i \mathbf{e}_i.$$

Similarly, the torque exerted by the  $i$ -th cable about the center of the receiver platform is

$$\tau_i = -t_i C(\mathbf{a}_i) \mathbf{e}_i.$$

By combining all cable forces and moments, the following matrix expression can be written:

$$\left[ \sum_{i=1}^6 \mathbf{f}_i \right] = - \begin{bmatrix} \mathbf{e}_1 & \dots & \mathbf{e}_6 \\ C(\mathbf{a}_1)\mathbf{e}_1 & \dots & C(\mathbf{a}_6)\mathbf{e}_6 \end{bmatrix} \begin{bmatrix} t_1 \\ \vdots \\ t_6 \end{bmatrix} = -\mathbf{J}^T \mathbf{T} \quad (8)$$

Here,  $\mathbf{T} = [t_1 \quad \dots \quad t_6]^T$  denotes the vector of cable tensions. Under static equilibrium and in the absence of external disturbances, the total cable force and torque must balance the gravitational force and moment induced by the platform's weight and its center-of-mass offset.

$$-\mathbf{J}^T \mathbf{T} + \mathbf{G} = \mathbf{0} \quad (9)$$

where  $\mathbf{G}$  denotes the resultant effect of gravity and the offset of the center of mass of the receiver platform. Its expression is given by:

$$\mathbf{G} = \left[ m \cdot C({}_P^O\mathbf{R} \cdot {}^P\mathbf{p}_m) \mathbf{g} \right].$$

Here,  $m$  denotes the total mass of the receiver platform,  ${}^P\mathbf{p}_m$  represents the position vector of the platform's center of mass in the receiver platform coordinate system, and the gravitational acceleration is taken as  $\mathbf{g} = [0 \quad 0 \quad -9.8]^T$  N/kg.

Through the above kinematic and static analysis of the new feed cabin structure, a comprehensive framework of coordinate systems, motion, and mechanical models has been established. This framework clarifies the intrinsic relationships among structural parameters, platform rotation angles, cable tension constraints, and gravitational forces, thereby providing a solid theoretical foundation for the subsequent optimization of structural parameters.

## Structural parameter optimization and performance validation

One of the primary objectives of the new configuration is to increase the tilt angle of the feed cabin to 50°. During the motion of the receiver platform, the tilting motion is dominant, serving to track signal sources, while also compensating for minor errors caused by the motion of the cabin truss. As the tilt angle varies, the tension of the cables correspondingly changes. At certain specific angles, the tension in one or more cables may suddenly drop, which can compromise the ability to effectively control the posture of the receiver platform. Therefore, based on the static mechanical model, the structural parameters need to be optimized with the maximum achievable tilt angle across all directions as the optimization target. This process also takes into account the constraints imposed by cable tension limits. The goal is to enhance the stability of the receiver platform under varying observation orientations.

### Polar coordinate search method

In the new configuration, the constraints and force distribution imposed by the six cables on the receiver platform remain within the scope described by the static equilibrium equations. The polar coordinate search method is used to evaluate the tilt capability. As shown in Fig. 7, the positive direction of the global X-axis is taken as the polar axis. The search direction is defined by a counterclockwise rotation from this axis, and the azimuth angle is denoted as  $\varphi_s$ . The tilt angle of the receiver platform along this direction is denoted as  $\varphi_p$ , representing a rotation about a unit vector  $n$  that is orthogonal to the search direction and aligned with the global Y-axis after being rotated about the Z-axis by  $\varphi_s$ .

For each azimuth direction  $\varphi_s$ , the platform tilt angle  $\varphi_p$  is incrementally increased with a fixed step of 0.1°. In each step, the cable tensions are computed according to the static equilibrium equations. The search in the current direction terminates once any cable tension reaches the prescribed safe working range of 1000–60000 N, which represents the physical operating limits of the system. The maximum attainable  $\varphi_p$  obtained in this process is recorded as the pitch capability in the corresponding azimuth direction. After sweeping all  $\varphi_s \in [0^\circ, 360^\circ]$ , the global pitch capability of the system is defined as the minimum value among all directions to ensure a conservative and robust evaluation.

To prevent numerical stagnation in regions where the tension variation is locally flat, a small perturbation of order  $10^{-3}$  is added to the azimuth update. This perturbation does not influence the final converged results; it only enhances numerical robustness. Since the algorithm performs a full sweep over  $\varphi_s \in [0^\circ, 360^\circ]$ , the method is inherently free from local optima.

The rotation matrix corresponding to a rotation about the unit vector  $n$  can be given by Rodrigues' rotation formula:

$$\mathbf{R}(\mathbf{n}, \varphi_p) = \mathbf{I} + \sin(\varphi_p)\mathbf{K} + (1 - \cos(\varphi_p))\mathbf{K}^2.$$

here,  $\mathbf{I}$  is the  $3 \times 3$  identity matrix, and  $\mathbf{K}$  is the skew-symmetric matrix associated with the unit vector  $\mathbf{n}$ :

$$\mathbf{K} = \begin{bmatrix} 0 & -n_z & n_y \\ n_z & 0 & -n_x \\ -n_y & n_x & 0 \end{bmatrix}.$$

The Rodrigues formula can also be used in reverse to determine the tilt angles of the receiver platform around the X, Y, and Z axes, yielding the corresponding rotation matrices  $\mathbf{R}_x$ ,  $\mathbf{R}_y$ , and  $\mathbf{R}_z$ . Following the rotation sequence of  $Z \rightarrow Y \rightarrow X$ , the overall rotation matrix can be expressed as:

$$\mathbf{R}(\mathbf{n}_z, \alpha_2) \cdot \mathbf{R}(\mathbf{n}_y, \beta_2) \cdot \mathbf{R}(\mathbf{n}_x, \gamma_2) = \mathbf{R}(\mathbf{n}, \varphi_p). \quad (10)$$

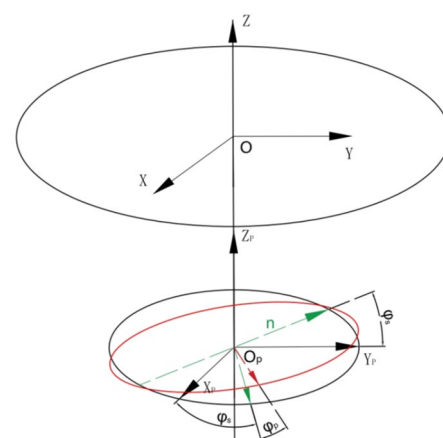


**Fig. 7.** Schematic diagram of tilt angle search.

By comparing both sides of the equation, the following rotation angles can be obtained, the rotation around the Y-axis is given by

$$\beta_2 = \arcsin(R_{13}),$$

the rotation around the X-axis by

$$\alpha_2 = \arccos\left(\frac{R_{33}}{\cos\beta_2}\right),$$

and the rotation around the Z-axis by

$$\gamma_2 = \arccos\left(\frac{R_{11}}{\cos\beta_2}\right),$$

where  $R_{ij}$  denotes the element in the  $i$ -th row and  $j$ -th column of the rotation matrix  $\mathbf{R}(\mathbf{n}, \varphi_p)$ . Accordingly, the relationship between the tilt angle  $\varphi_p$  and the cable tension vector  $\mathbf{T} = [t_1 \dots t_6]^T$  is established.

### Structural parameter optimization

According to prior knowledge and based on the mechanism design and data fitting in astronomical observation<sup>14</sup>, the relationship between the tilt angle of the cabin truss  $\varphi_B$  and the zenith angle  $\varphi$  is given in Equation (11). The cabin truss is capable of achieving tilt angles ranging from  $0^\circ$  to  $13.5^\circ$ . To enable the feed cabin to reach a tilt angle of  $50^\circ$ , the receiver platform must achieve a maximum tilt angle of at least  $36.5^\circ$ . To enable the feed cabin to smoothly transition across zenith angles ranging from  $0^\circ$  to  $50^\circ$ , it is essential to comprehensively consider multiple geometric and kinematic parameters of both the cabin truss and receiver platform. These parameters directly affect the pitch capability of the receiver platform and the observable sky area of FAST. Therefore, this section utilizes simulation-based analysis to investigate the influence of various parameter configurations on the maximum achievable tilt angle and performs optimization on the key structural parameters. Table 1 lists the value ranges of all critical parameters.

$$\varphi_B = \begin{cases} \frac{3}{8}\varphi, & 0^\circ \leq \varphi \leq 30^\circ \\ -\frac{21}{1600}\varphi^2 + \frac{93}{80}\varphi - \frac{189}{16}, & 30^\circ < \varphi < 90^\circ \end{cases} \quad (11)$$

- Optimization of Adjacent Winch and Anchor Point Angles

To analyze the impact of the angle between the adjacent winches and the anchor points on the pitch capability of the receiver platform, an angular nested loop method is employed. By progressively adjusting the angle values, the effect on the maximum achievable tilt angle is evaluated. Specifically, a parametric search is conducted within the range of  $[0^\circ, 60^\circ]$  for the angles  $\varphi_1$  and  $\varphi_2$  defined in the cabin truss coordinate system. The goal is to determine how variations in these angles influence the maximum tilt angle that the receiver platform can achieve in various directions. In the preliminary simulation, referring to the receiver dimensions shown in Fig. 3, the initial vertical offset between the cabin truss and the receiver platform is set as  $p_z = -2$  m, and the anchor-point radius is set as  $r_2 = 2.1$  m.

The results, as shown in Fig. 8, indicate that when both angles  $\varphi_1$  and  $\varphi_2$  are close to  $0^\circ$ , the receiver platform achieves its maximum pitch capability. As either of the angles increases, the pitch performance of the platform gradually deteriorates. This decline is attributed to the increased angle between adjacent winches and anchor points, which leads to greater differences in tension among the cables. When both angles approach  $60^\circ$ , the receiver platform gradually loses its pitch capability, as shown in Fig. 9(b). Under such angular configurations, the cable tension distribution becomes highly uneven, and some cables exhibit near-zero tension even at small

Parameter name	Symbol	Value range
Cable tension limits	$F_{\min, \max}$	(1000, 60000) N
Tilt angle range	$\text{Angle}_{\min, \max}$	( $0^\circ$ , $50^\circ$ )
Vertical distance between cabin truss and receiver platform	$p_z$	[ $-3$ , $-1$ ] m
Winch distribution radius	$r_1$	3.5 m
Anchor point distribution radius	$r_2$	[1.5, 2.5] m
Receiver platform mass	$m$	4500 kg
Adjacent winch angle	$\varphi_1$	[ $0$ , $60^\circ$ ]
Adjacent anchor point angle	$\varphi_2$	[ $0$ , $60^\circ$ ]

**Table 1.** Structural parameter ranges of the feed cabin system.

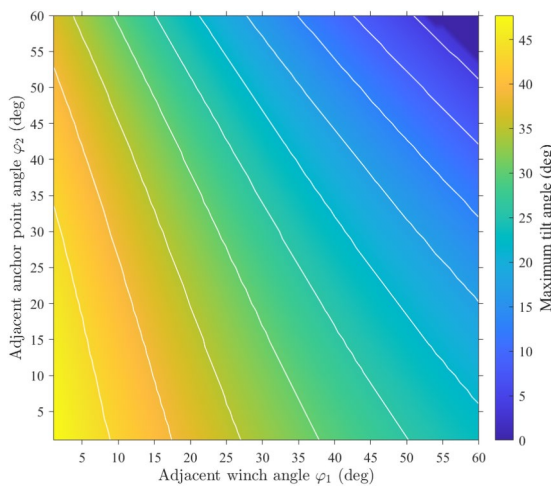


**Fig. 8.** Relationship between receiver platform radius and maximum tilt angle.

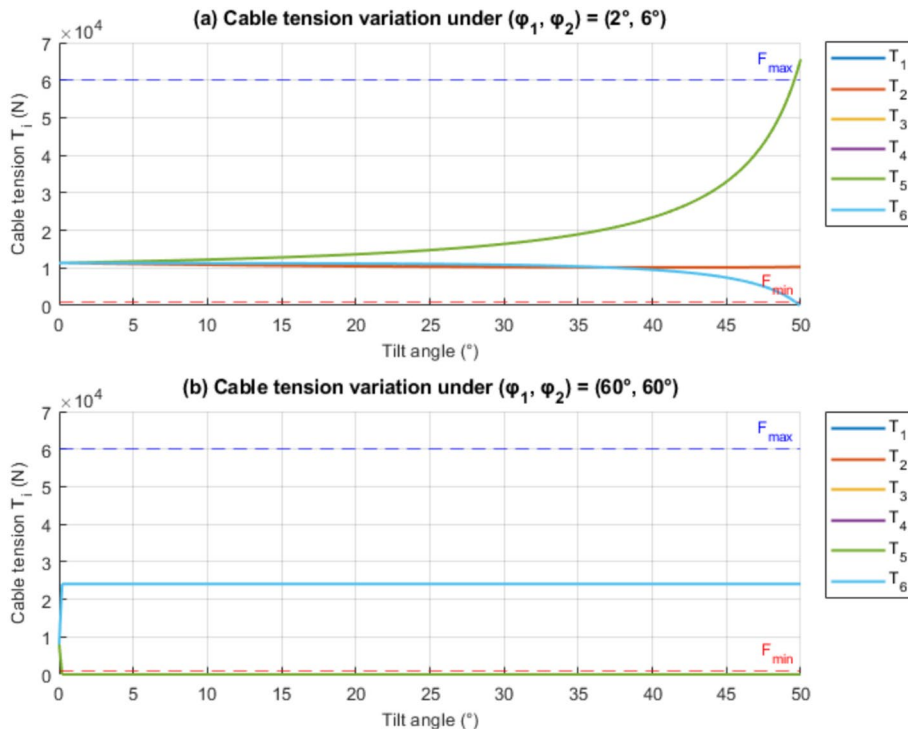


**Fig. 9.** Cable tension under different geometric configurations.

tilt angles. This indicates that the system's overall tension equilibrium is no longer sustainable. Consequently, the Jacobian matrix governing the tension–motion relationship approaches a near-singular state, leading to mechanical instability and a loss of effective pitch adjustment capability.

Considering the spatial constraints of the winches and the anchor points in practical applications, the optimized angles are selected as  $\varphi_1 = 2^\circ$  and  $\varphi_2 = 6^\circ$ . This selection not only ensures structural stability but also preserves sufficient pitch capability to meet the zenith angle requirements in real operational scenarios.

- Optimization of Receiver platform Radius and Platform Distance

After optimizing  $\varphi_1$  and  $\varphi_2$ , other parameters are held constant to further analyze the influence of the receiver platform radius  $r_2$  on the maximum achievable tilt angle. Simulations are conducted with  $r_2$  varying within the range of [1.5, 2.5] m, and the results are shown in Fig. 10. As the receiver platform radius increases, the tilting capability of the system improves accordingly. Therefore,  $r_2 = 2.5$  m is selected as the recommended value.

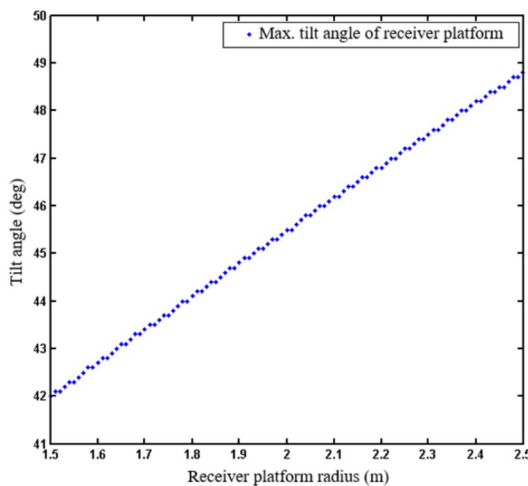


**Fig. 10.** Relationship between receiver-platform radius and maximum tilt angle.

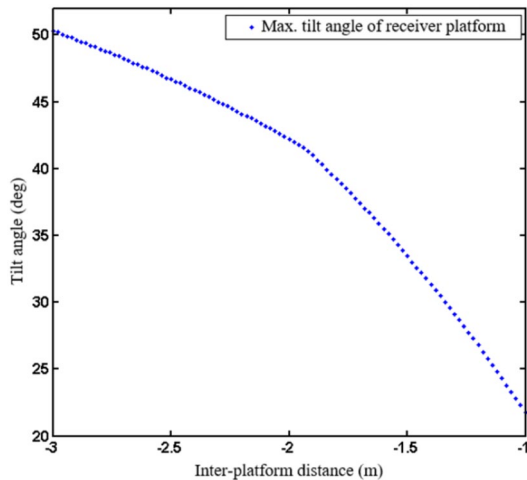


**Fig. 11.** Relationship between inter-platform distance and maximum tilt angle.

Subsequently, based on the optimized parameters, the influence of the vertical distance  $p_z$  between the receiver platform and the cabin truss is analyzed. A parameter sweep is conducted over  $p_z \in [-3, -1]$  m to determine the maximum achievable tilt angle. As shown in Fig. 11, the tilting capability improves as the receiver platform moves further away from the cabin truss. As the inter-platform distance  $p_z$  increases, the directional differences among the six cables become smaller, reducing tension coupling and allowing the cable forces to remain more evenly balanced, which enhances the overall tilting performance. However, the selection of  $p_z$  must also consider the spatial requirements for accommodating the receiver instruments. Based on this trade-off, the final value is chosen as  $p_z = -2.5$  m, which provides both sufficient tilting capability and adequate installation space.

- Optimization of Center of Mass Position

After optimizing the geometric parameters of the receiver platform, further analysis is conducted on the effect of the center-of-mass offset on the platform's pitch capability. The center-of-mass vector of the receiver system is defined in the receiver platform coordinate system  $\{P\}$  as  $\mathbf{p}_m = [p_{mx}, p_{my}, p_{mz}]^T$ . During this analysis, only the horizontal components ( $p_{mx}, p_{my}$ ) are varied, while the vertical component is fixed at  $p_{mz} = 0$ , corresponding to the mid-plane of the receiver platform.

As shown in Fig. 12, when the center of mass of the receiver platform is offset within the X-Y plane along  $\varphi_s = 0^\circ$  and  $\varphi_s = 120^\circ$ , the platform exhibits the following trend: When tilting in the same direction as the center-of-mass offset, the platform's tilt capability is enhanced due to an additional tilting moment generated by the offset, which assists the tilting motion. Conversely, when tilting opposite to the offset direction, the performance is diminished as the offset introduces a counteracting moment, requiring higher cable tension and reducing the attainable tilt angle in that direction.

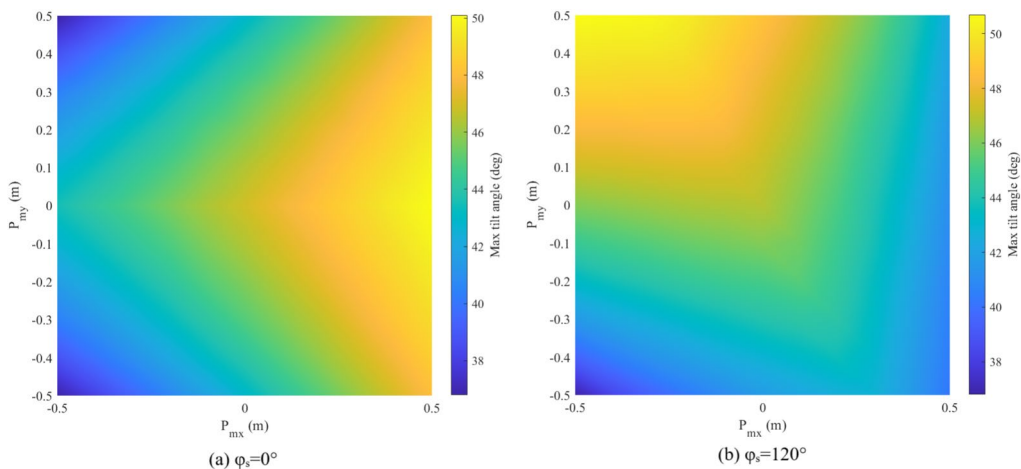


**Fig. 12.** Relationship between the horizontal center of mass of the receiver platform and the tilt angle.

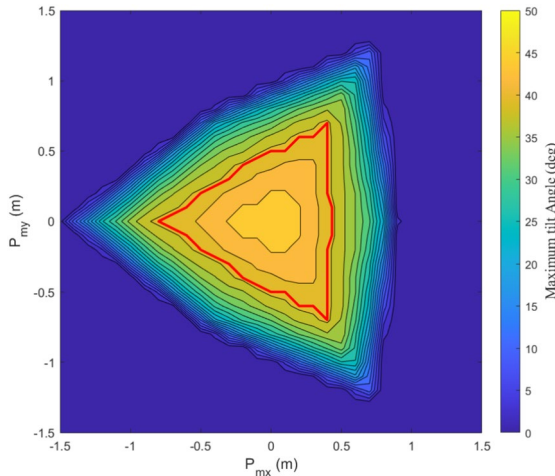


**Fig. 13.** Relationship between center-of-mass offset and tilt angle.

Serial number	Receiver name	Dimensions (m)	Height (m)	Weight (kg)
1	450M Receiver	0.7	0.5	30
2	PAF Multi-beam	2.1	2.0	1200
3	L-band 19-Beam	1.8	1.6	1200
4	Ultra-wideband Receiver	1.0	1.2	200
5	S-band Multi-beam	1.2	1.2	150
6	Test Platform	1.5	0.5	500

**Table 2.** Receiver platform layout diagram.

Building upon this directional analysis, a comprehensive parametric sweep is performed to evaluate the platform's maximum tilt angle under center-of-mass offsets in all directions within the X-Y plane. The feasible region is defined as the area where the minimum tilt angle, evaluated across all orientations at each offset point, exceeds  $36.5^\circ$ , as illustrated in Fig. 13.

Based on the receiver configuration shown in Table 2 and Fig. 3, the computed center of mass of the current layout is  $[-0.0076, -0.1548]$ , which lies well within the feasible region. This demonstrates that the proposed receiver configuration satisfies the tilt angle requirements under asymmetric mass distribution. Furthermore, since the feasible region characterizes all center-of-mass offsets that maintain sufficient tilt capability, future receiver configurations will also remain compliant as long as their resulting center of mass falls within this region. Thus, the presented analysis provides general guidance for future payload updates on the receiver platform.

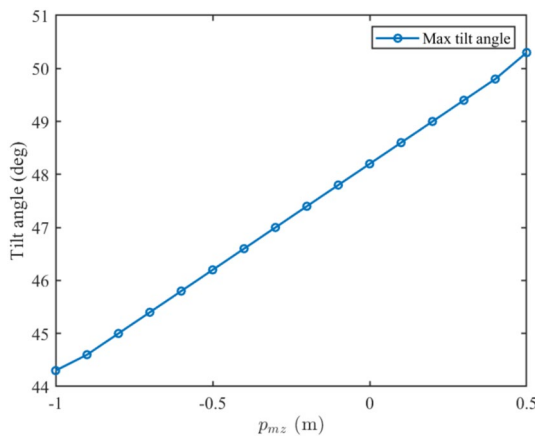


**Fig. 14.** Relationship between vertical center of gravity and maximum tilt angle of the receiver platform.

Parameter description	Symbol	Value
Vertical offset between truss center and receiver platform center (along $Z_B$ )	$p_z$	-2.5 m
Winch distribution radius	$r_1$	3.5 m
Anchor point distribution radius	$r_2$	2.5 m
Adjacent winch angle	$\varphi_1$	2°
Adjacent anchor point angle	$\varphi_2$	6°

**Table 3.** Optimized structural parameters of the feed cabin system.

Next, within the receiver platform coordinate system  $\{P\}$ , the height of the center of mass is varied along the  $Z_P$ -axis in the range  $p_{mz} \in [-1, 0.5]$  m. The simulation results are shown in Fig. 14. It can be observed that, under a fixed inter-platform distance  $p_z = -2.5$  m, a moderate upward shift of the center of mass (i.e., increasing  $p_{mz}$ ) enhances the maximum achievable tilt angle. This improvement arises because a higher center of mass increases the gravitational moment that assists the tilting motion within the allowable cable tension range.

It should be emphasized that this behavior does not contradict the earlier result that increasing the inter-platform distance  $p_z$  improves tilt capability. The two parameters govern different physical aspects:  $p_z$  shapes the geometric configuration and cable layout between the truss and the platform, whereas  $p_{mz}$  reflects only the internal mass distribution of the platform. In practice,  $p_{mz}$  may be raised slightly to enhance the gravitational moment that assists tilting, but only within a limited range to ensure overall stability. A balanced design should therefore adopt a sufficiently large inter-platform distance  $p_z$  together with a moderately elevated, well-controlled center-of-mass height  $p_{mz}$ .

This section conducts a parametric analysis of key geometric variables of both the cabin truss and the receiver platform. Based on the simulation results, a set of suitable parameter values is selected, as summarized in Table 3. These recommended parameters ensure that the receiver platform achieves the required tilt capability for a zenith angle range of 0° to 50°, while maintaining satisfactory structural stability. To further confirm the reliability of the selected configuration, several initial parameter sets within the prescribed ranges were tested, and all cases converged to the same results. This demonstrates that the final parameter selection is independent of the initial values and that the global scanning method is deterministic and stable. The resulting parameter configuration provides a solid basis for subsequent performance evaluation and practical engineering implementation.

## Tilt and payload performance validation of the feed cabin system

### Tilt performance verification

Under the optimized structural parameters, the maximum tilt angle of the receiver platform along a full azimuth rotation was calculated. As shown in Fig. 15, the distribution of the maximum tilt angle is illustrated in a 3D Cartesian coordinate system. Point O represents the center of the receiver platform, and the Y-axis is aligned with  $Y_P$  of the receiver platform coordinate system. The red circle represents the receiver platform (not to scale). The Z-axis indicates the maximum tilt angle of the receiver platform in each azimuth direction, measured in degrees. It can be observed that the minimum value of the maximum tilt angle across all directions is 41.9°, which satisfies the tilt angle requirement of the receiver platform.

The receiver platform achieves notably large tilt angles in the directions of  $\varphi_s = 60^\circ, 180^\circ$ , and  $300^\circ$ . However, in these directions, even minor angular deviations of the platform lead to significant fluctuations in both the tilt angle and cable tension. This behavior introduces risks such as slack cables or loss of control, making these extreme values impractical for real application. Considering the need for operational stability, it is more

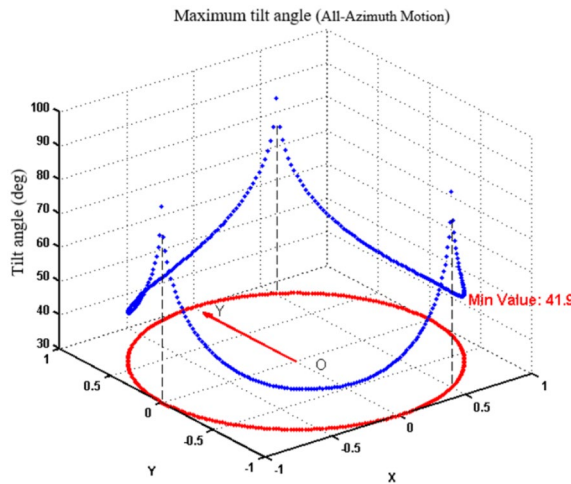


**Fig. 15.** Max tilt angle of the receiver platform (all-azimuth motion).

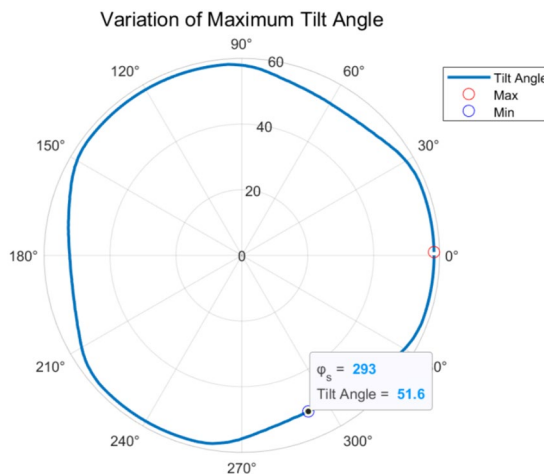


**Fig. 16.** Maximum zenith angle (all-azimuth motion).

appropriate to adopt the minimum value of the maximum tilt angle across all directions as the evaluation metric for tilt capability. This conservative but robust criterion ensures that the platform maintains reliable control performance under various observational orientations.

To further evaluate the overall performance of the new configuration, the maximum achievable tilt angle of the feed cabin was analyzed under coordinated motion of the cabin truss and the receiver platform in the same direction. A full-angle search over  $\varphi_s \in [0^\circ, 360^\circ]$  was conducted, with an additional constraint imposed during the evaluation: the difference between the maximum and minimum cable tensions must remain smaller than the total gravitational force of the receiver platform, that is,

$$\max(T_i) - \min(T_i) < mg, \quad (12)$$

where  $T_i$  denotes the tension in the  $i$ -th cable, and  $mg$  is the total gravitational force acting on the receiver platform. This constraint is derived from the static force characteristics of six-cable parallel mechanisms. Since  $mg$  represents a typical load scale of the system, restricting the tension difference within this magnitude prevents any single cable from deviating excessively from the others. This avoids entering a single-cable-dominant loading mode, which could otherwise lead to slack cables or instability in the attitude control of the receiver platform.

This constraint is intended to suppress sharp variations in tilt angle and cable tension in certain specific directions, as well as to enhance the overall stability and coordination of the system.

The simulation results, including the distribution of tilt angles and cable tension variations, are presented in Figs. 16 and 17. It is observed that the minimum value among the maximum tilt angles across all directions reaches  $51.6^\circ$ , fulfilling the design requirement of achieving a  $50^\circ$  zenith angle. Further analysis shows that the cable tensions remain within acceptable limits and vary smoothly throughout the process, confirming both the structural stability and the feasibility of the proposed configuration.

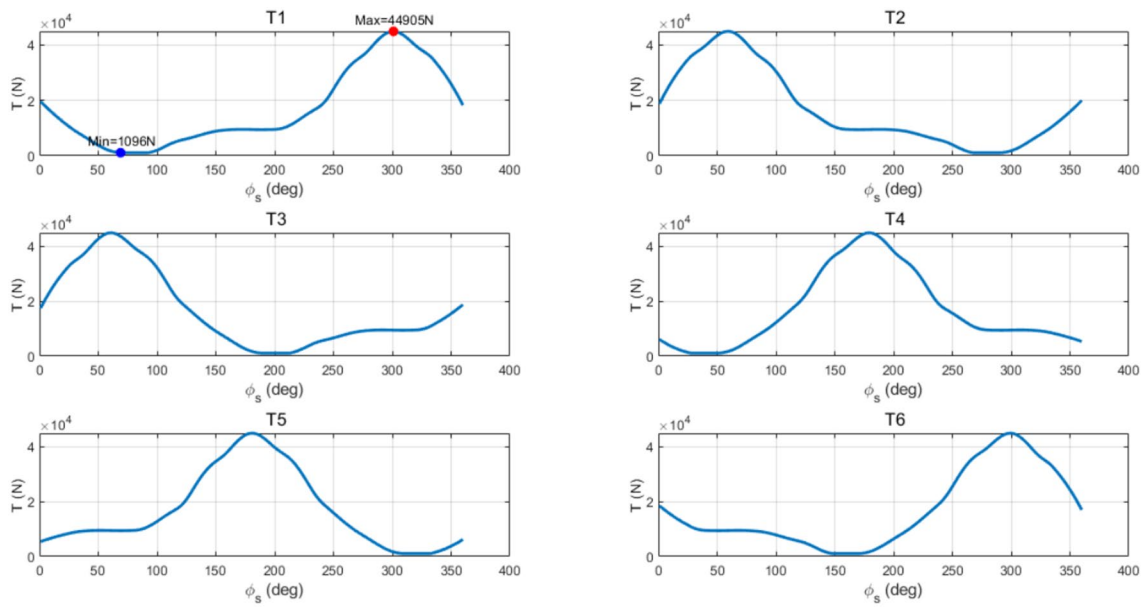


**Fig. 17.** Cable tension variation.

### Payload capacity enhancement

To assess the engineering feasibility of the new feed cabin structure, a comparative analysis was conducted on the overall mass distribution and payload capacity of the internal feed support system. In the original design, the A–B rotator mechanism and the Stewart platform together weighed approximately 10.1 tons, while for most of the operational time, they carried only a single 19-beam L-band receiver with a mass of about 1200 kg. In contrast, the cable-driven fine-tuning mechanism proposed in this study weighs only about 3 tons. Within the same overall feed cabin structural mass budget, it is capable of supporting up to six receivers operating across different frequency bands, with a total payload capacity of up to 3280 kg—approximately a 173% increase compared to the original single-receiver capacity. Moreover, despite the significant increase in payload, the overall structural mass is reduced by more than 5 tons. These results demonstrate the significant advantages of the new structure in terms of weight reduction and enhanced observational performance.

### Conclusion

In this paper, the influence of the feed cabin's structural parameters on the system's zenith angle coverage and receiver payload capacity was systematically investigated. The main conclusions are summarized as follows:

1. The optimized structural parameters meet the spatial requirements for receiver installation and significantly enhance the payload capacity of the receiver platform. Under the premise of ensuring structural safety and stability, the system can support the integration of multiple types of receivers.
2. The minimum zenith angle reaches the target value of  $50^\circ$ , fulfilling the observation requirements of the upgraded feed cabin configuration. Meanwhile, the cable tension remains within a reasonable range and changes smoothly, validating the operational stability and engineering feasibility of the proposed system.

The new feed cabin configuration scheme will effectively expand the observation zenith angle range while ensuring system safety and stability, providing feasible theoretical support and practical foundation for the subsequent upgrades of FAST. Future work will further integrate experimental validation and control system design to promote the application and deployment of this solution in real-world engineering.

### Data availability

The datasets generated or analyzed during the current study that support the reproducibility of the experiments and the validation of the models are available from LuCong Zhang ([lczhang.bao.ac.cn](http://lczhang.bao.ac.cn)) upon reasonable request.

Received: 19 August 2025; Accepted: 2 December 2025

Published online: 25 December 2025

### References

1. Nan, R. Five hundred meter aperture spherical radio telescope (fast). *Sci. China series G* **49**, 129–148. <https://doi.org/10.1007/s11433-006-0129-9> (2006).
2. Nan, R. et al. The five-hundred-meter aperture spherical radio telescope (fast) project. *Int. J. Mod. Phys. D* **20**, 989–1024. <https://doi.org/10.1142/S0218271811019335> (2011).
3. Jiang, P. et al. Commissioning progress of the fast. *Sci. China Physics, Mech. & Astron.* **62**, 959502. <https://doi.org/10.1007/s11433-018-9376-1> (2019).
4. Luo, R. et al. Diverse polarization angle swings from a repeating fast radio burst source. *Nature* **586**, 693–696. <https://doi.org/10.1038/s41586-020-2827-2> (2020).

5. Zhang, B. The physical mechanisms of fast radio bursts. *Nature* **587**, 45–53. <https://doi.org/10.1038/s41586-020-2828-1> (2020).
6. Lin, L. et al. No pulsed radio emission during a bursting phase of a galactic magnetar. *Nature* **587**, 63–65. <https://doi.org/10.1038/s41586-020-2839-y> (2020).
7. Yao, J. et al. The first evidence for three-dimensional spin-velocity alignment in pulsars. arXiv preprint [arXiv:2103.01839](https://arxiv.org/abs/2103.01839)<https://doi.org/10.48550/arXiv.2103.01839> (2021).
8. Li, D. et al. A bimodal burst energy distribution of a repeating fast radio burst source. *Nature* **598**, 267–271. <https://doi.org/10.1038/s41586-021-03878-5> (2021).
9. Qian, L. et al. Fast: its scientific achievements and prospects. *The Innov.* **1**, <https://doi.org/10.1016/j.xinn.2020.100053> (2020).
10. Jiang, P., Shen, Z.-Q. & Xu, R.-X. Preface: Key technologies for enhancing the performance of fast. *Res. Astron. Astrophys* **20**, 063. <https://doi.org/10.1088/1674-4527/20/5/63> (2020).
11. Yin, J.-N., Jiang, P. & Yao, R. An approximately analytical solution method for the cable-driven parallel robot in fast. *Res. Astron. Astrophys* **21**, 046. <https://doi.org/10.1088/1674-4527/21/2/46> (2021).
12. Jiang, P. et al. The fundamental performance of fast with 19-beam receiver at l band. *Res. Astron. Astrophys* **20**, 064. <https://doi.org/10.1088/1674-4527/20/5/64> (2020).
13. Tang, X., Zhu, W., Sun, C. & Yao, R. Similarity model of feed support system for fast. *Exp. Astron.* **29**, 177–187. <https://doi.org/10.1007/s10686-010-9211-4> (2011).
14. Yin, J., Jiang, P. & Yao, R. Pose optimization of the fast feed support system based on the new feed cabin mechanism. *Sci. China Physics, Mech. & Astron.* **66**, 239513. <https://doi.org/10.1007/s11433-022-1997-8> (2023).
15. Yao, R., Jiang, P. & Yang, Q. A fast feed cabin positioning mechanism. China Patent CN213517737U, Published June 22, 2021 (2021).
16. Yin, J., Yao, R. & Jiang, P. Mechanical modeling and optimization for the new improved configuration of the fast feed cabin. *J. Phys.: Conf. Ser.* **3022**, 012015. <https://doi.org/10.1088/1742-6596/3022/1/012015> (2025).

## Author contributions

J.H.S. and L.C.Z. conceived the study. J.H.S., H.L. and P.J. provided the research data and funding support. L.C.Z. performed the modelling, simulation experiments, and drafted the manuscript. J.H.S. and H.L. revised the manuscript. All authors reviewed the manuscript.

## Funding

This work was supported by the Guizhou Provincial Science and Technology Projects (No. QKHPTRC-ZDSYS[2023]003).

## Declarations

### Competing interests

The authors declare no competing interests.

### Additional information

**Correspondence** and requests for materials should be addressed to J.S.

**Reprints and permissions information** is available at [www.nature.com/reprints](http://www.nature.com/reprints).

**Publisher's note** Springer Nature remains neutral with regard to jurisdictional claims in published maps and institutional affiliations.

**Open Access** This article is licensed under a Creative Commons Attribution-NonCommercial-NoDerivatives 4.0 International License, which permits any non-commercial use, sharing, distribution and reproduction in any medium or format, as long as you give appropriate credit to the original author(s) and the source, provide a link to the Creative Commons licence, and indicate if you modified the licensed material. You do not have permission under this licence to share adapted material derived from this article or parts of it. The images or other third party material in this article are included in the article's Creative Commons licence, unless indicated otherwise in a credit line to the material. If material is not included in the article's Creative Commons licence and your intended use is not permitted by statutory regulation or exceeds the permitted use, you will need to obtain permission directly from the copyright holder. To view a copy of this licence, visit <http://creativecommons.org/licenses/by-nc-nd/4.0/>.

© The Author(s) 2025